

Central Lancashire Online Knowledge (CLoK)

Title	Synthesis of carbon-13 labelled carbonaceous deposits and their evaluation for potential use as surrogates to better understand the behaviour of the carbon-14-containing deposit present in irradiated PGA graphite
Type	Article
URL	https://clok.uclan.ac.uk/id/eprint/13924/
DOI	https://doi.org/10.1016/j.jnucmat.2015.12.021
Date	2016
Citation	Payne, L, Walker, S., Bond, G., Eccles, Harry, Heard, P.J., Scott, T.B. and Williams, S.J. (2016) Synthesis of carbon-13 labelled carbonaceous deposits and their evaluation for potential use as surrogates to better understand the behaviour of the carbon-14-containing deposit present in irradiated PGA graphite. Journal of Nuclear Materials, 470. pp. 268-277. ISSN 0022-3115
Creators	Payne, L, Walker, S., Bond, G., Eccles, Harry, Heard, P.J., Scott, T.B. and
	Williams, S.J.

It is advisable to refer to the publisher's version if you intend to cite from the work. https://doi.org/10.1016/j.jnucmat.2015.12.021

For information about Research at UCLan please go to http://www.uclan.ac.uk/research/

All outputs in CLoK are protected by Intellectual Property Rights law, including Copyright law. Copyright, IPR and Moral Rights for the works on this site are retained by the individual authors and/or other copyright owners. Terms and conditions for use of this material are defined in the http://clok.uclan.ac.uk/policies/

Accepted Manuscript

Synthesis of carbon-13 labelled carbonaceous deposits and their evaluation for potential use as surrogates to better understand the behaviour of the carbon-14-containing deposit present in irradiated PGA graphite

L. Payne, S. Walker, G. Bond, H. Eccles, P.J. Heard, T.B. Scott, S.J. Williams



PII: S0022-3115(15)30390-1

DOI: 10.1016/j.jnucmat.2015.12.021

Reference: NUMA 49514

To appear in: Journal of Nuclear Materials

Received Date: 6 April 2015

Revised Date: 15 December 2015 Accepted Date: 18 December 2015

Please cite this article as: L. Payne, S. Walker, G. Bond, H. Eccles, P.J. Heard, T.B. Scott, S.J. Williams, Synthesis of carbon-13 labelled carbonaceous deposits and their evaluation for potential use as surrogates to better understand the behaviour of the carbon-14-containing deposit present in irradiated PGA graphite, *Journal of Nuclear Materials* (2016), doi: 10.1016/j.jnucmat.2015.12.021.

This is a PDF file of an unedited manuscript that has been accepted for publication. As a service to our customers we are providing this early version of the manuscript. The manuscript will undergo copyediting, typesetting, and review of the resulting proof before it is published in its final form. Please note that during the production process errors may be discovered which could affect the content, and all legal disclaimers that apply to the journal pertain.

- 1 Synthesis of carbon-13 labelled carbonaceous deposits and their
- 2 evaluation for potential use as surrogates to better understand the
- 3 behaviour of the carbon-14-containing deposit present in
- 4 irradiated PGA graphite.
- 5 L. Payne^{a*}, S. Walker^b, G. Bond^b, H. Eccles^c, P. J. Heard^a, T. B. Scott^a and S. J.
- 6 Williams^d.
- a) Interface Analysis Centre, HH Wills Physics Laboratory, University of Bristol, BS8 1TL, UK.
- 8 b) Centre for Materials Science, University of Central Lancashire, PR1 2HE, UK.
- 9 c) John Tyndall Institute for Nuclear Research, School of Computing, Engineering and Physical
- 10 Sciences, University of Central Lancashire, PR1 2HE, UK.
- d) Radioactive Waste Management, B587, Curie Avenue, Harwell Oxford, Didcot, OX11 0RH, UK
- 12 Abstract
- 13 The present work has used microwave plasma chemical vapour deposition to generate
- suitable isotopically labelled carbonaceous deposits on the surface of Pile Grade A graphite
- for use as surrogates for studying the behaviour of the deposits observed on irradiated
- graphite extracted from UK Magnox reactors. These deposits have been shown elsewhere to
- 17 contain an enhanced concentration of ¹⁴C compared to the bulk graphite. A combination of
- 18 Raman spectroscopy, ion beam milling with scanning electron microscopy and secondary ion
- mass spectrometry were used to determine topography and internal morphology in the formed
- 20 deposits. Direct comparison was made against deposits found on irradiated graphite samples
- 21 trepanned from a Magnox reactor core and showed a good similarity in appearance. This
- 22 work suggests that the microwave plasma chemical vapour deposition technique is of value in
- producing simulant carbon deposits, being of sufficiently representative morphology for use
- in non-radioactive surrogate studies of post-disposal behaviour of ¹⁴C-containing deposits on
- some irradiated Magnox reactor graphite.

26 27

28

29

- 31 *Corresponding author. Tel.: +44 (0) 117 331 17683
- 32 Email address: liam.payne@bristol.ac.uk (L. Payne)

1. Introduction

34	The decommissioning of the UK's first generation of gas-cooled, graphite-moderated
35	(Magnox) reactors will lead to approximately 45,000 m ³ of irradiated reactor core graphite,
36	with a packaged volume of 59,000 m ³ , for geological disposal [1]. An important radionuclide
37	in safety assessments for the disposal of radioactive waste in a geological disposal facility
38	(GDF) is the long lived isotope ¹⁴ C (half-life 5730 years) [2]. With an approximate total ¹⁴ C
39	activity of more than 7000 TBq arising from Magnox graphite cores and the additional
40	volume of graphite waste arising from advanced gas-cooled reactors (AGR) [2], investigation
41	of the behaviour of ¹⁴ C associated with such wastes after closure of a geological disposal
42	facility is important. Whilst reactor graphite has been extensively studied from a physio-
43	mechanical standpoint, related to core integrity, relatively little research effort has been
44	placed on understanding the behaviour of the graphite and constituent ¹⁴ C in a geological
45	disposal environment.
46	Recent research [3] providing post mortem analysis of irradiated graphite from two Magnox
47	reactor cores highlighted the presence of a carbonaceous deposit on the exposed surfaces of
48	the graphite bricks (channel and interstitial walls) from one of the reactors that has a
49	pronounced and markedly different morphology to the bulk graphite. The extent of this
50	deposit is likely to be a worst case scenario and it is anticipated that not all Magnox reactors
51	may contain such significant deposits. However, these surface deposits have been determined
52	to have a significant ¹⁴ C content compared to the bulk graphite [4] that has been created via
53	formation pathways discussed elsewhere [5]. It is not understood how these deposits will
54	behave in a GDF setting in comparison to the graphite which it coats. Specifically there is a
55	gap in the understanding of the release rate and magnitude of the labile ¹⁴ C fraction, of which
56	¹⁴ C located in deposited material may contribute significantly, with this labile fraction
57	expected to achieve relatively early release in the lifetime of a GDF [6]. The pronounced
58	"cauliflower-like" morphology observed is not unique to nuclear reactors and similar
59	morphologies have been commonly reported within the scientific literature for carbon from a
60	range of deposition techniques unrelated to nuclear applications [7-11]. At present such
61	deposits are of specific interest in geological disposal of graphite waste from the
62	decommissioning of Magnox reactors, as the deposited material may be present and represent
63	a significant fraction of the labile ¹⁴ C.
64	The Magnox reactors represent the first generation of gas-cooled reactors in the UK that used
65	carbon dioxide (CO ₂) as the primary coolant and a honeycomb network of graphite bricks to

66	provide neutron moderation. During reactor operation significant amounts of carbon
67	monoxide (CO) was produced from the CO_2 coolant. This CO in turn can be radiolytically
68	polymerised to form a carbonaceous deposit on free surfaces [12]. This non-graphitic carbon
69	deposit is significantly more chemically reactive to air than the underlying graphite [12, 13].
70	During the lifetime of some Magnox reactors, small quantities of methane gas were injected
71	into the coolant gas to inhibit weight loss of the graphite core due to radiolytic oxidation [14].
72	Methane (CH ₄) is a precursor for carbonaceous deposits that form a sacrificial layer
73	protecting the underlying graphite from excessive weight loss [15] and reduction in
74	mechanical strength [16]. It is assumed nitrogen incorporation during deposit formation is the
75	subsequent production route for the high ¹⁴ C levels observed.
76	CH ₄ is also a commonly utilised feedstock gas for the production of diamond and other
77	carbon coatings by the process of chemical vapour deposition (CVD) [17]. The growth of
78	carbon materials by CVD involves the excitation of a carbon-containing precursor gas using a
79	thermal or plasma energy source that creates activated radicals that will bond to a suitable
80	exposed surface. Therefore, even though differences exist in the formation of carbonaceous
81	deposits from CO and CH ₄ , both include the activation of carbon-containing gas creating
82	activated carbon species that will bond to surfaces. Recent work [3] showed that graphite
83	from the Oldbury Magnox power station, which had methane introduced into the coolant gas,
84	had a significant deposit on the fuel and interstitial channel walls of the graphite bricks. This
85	suggested that the deposit formed may be due to methane. A comparison of the morphology
86	and density of such deposits will help determine whether a ¹³ C methane deposit can be used
87	as a simulant for the surface deposit found on irradiated graphite in further work. If $^{13}\mathrm{C}$
88	carbonaceous deposits can be used as a simulant for the deposits seen on irradiated graphite it
89	will allow easier, non-radioactive investigations of the potential release of ¹⁴ C from deposits
90	on irradiated graphite in a geological disposal environment including the potential microbial
91	interaction with such material. If the deposits observed on the graphite behave differently to
92	the underlying graphite it may lead to a significantly different release rate for ¹⁴ C from the
93	deposit than from the underlying graphite when contacted by groundwater some time after
94	the closure of a geological disposal facility. Microbial colonisation may also be more likely
95	on the deposit than the underlying graphite due to the increased surface area due to the
96	amorphous nature of the material.
97	The use of a ¹³ C simulant allows wider access into the research of nuclear graphite, which
98	contains many other radionuclides such as ⁶⁰ Co, as facilities to handle radioactive materials
99	are not required. Isotopic differences in the precursor material should not alter the chemical

nature and/or effect the chemistry of the deposited carbon material. To this end, ¹³C has previously been used as a common isotopic tracer in biological systems [18] and implanted in graphite [19] as a non-radioactive proxy for ¹⁴C. In the current work we demonstrate the use of microwave plasma CVD to create a carbonaceous layer on graphite substrates that exhibit similar morphologies and densities to deposits observed to have formed in-service on Magnox graphite moderator blocks. The non-radioactive isotope ¹³C was selected as a tracer during CVD deposition such that deposit-substrate interfaces could be clearly resolved using imaging mass spectrometry analysis to determine the degree of material mixing and substrate etching.

The present work is part of a larger programme (C14-BIG) directed at gaining a better understanding and predicting the release of graphite derived ¹⁴C from a GDF and the influence of microbial activity under alkaline conditions expected to predominate for a significant time in a cement-based near field of a geological disposal facility after closure.

2. Experimental

2.1. Sample preparation

Pile Grade A (PGA) graphite was provided by Magnox Limited as a surplus material from the commissioning of the Wylfa nuclear power reactors, Wales. This graphite was trepanned into cores of 12 mm diameter using a stainless steel coring tool. The cores were then cut into 2 mm thick discs using a South Bay Technology Inc. Model 650 low speed diamond cutting wheel with deionised water used as coolant. This process gave a flat surface that was a

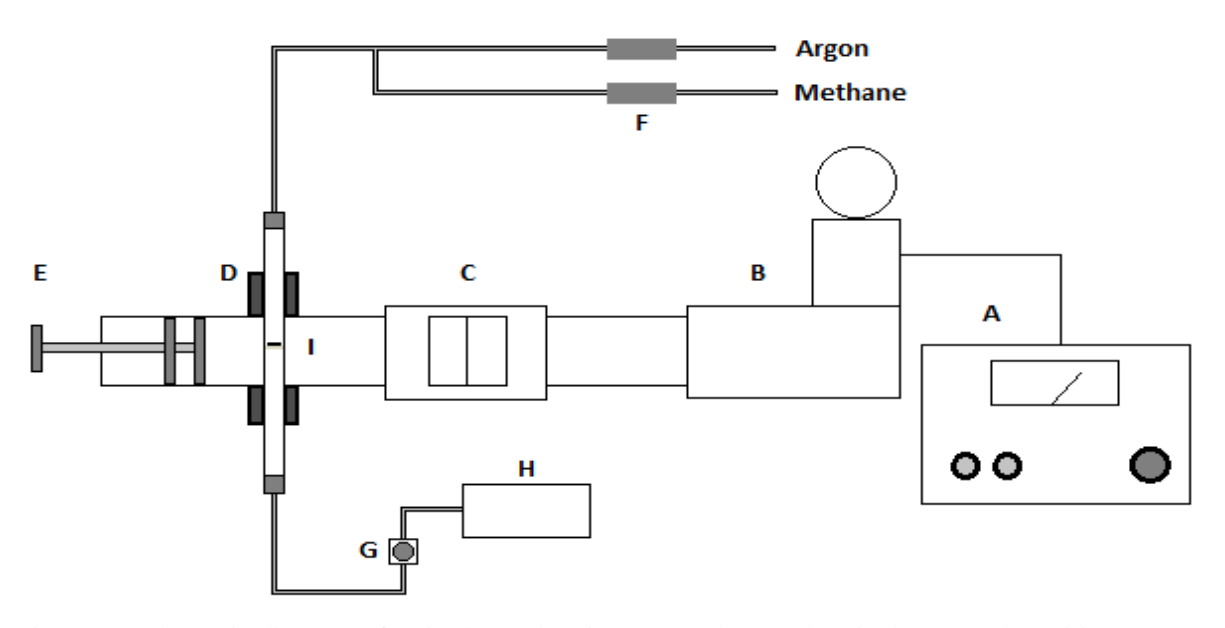


Figure 1, Schematic diagram of a single mode microwave plasma chemical vapour deposition (MPCVD) system. (A: variable power microwave controller (max. 1000 W); B: air-cooled microwave generator; C: water-cooled circulator; D: 4 port single mode TE01 microwave cavity; E: double plunge microwave tuner; F: mass-flow controllers; G: diaphragm vacuum pump; H: mass spectrometer; I: quartz tube containing a graphite disc on a porous glass sinter.)

120	suitable substrate for deposition. Subsequently ¹² C and ¹³ C carbonaceous deposits were
121	formed on the graphite surfaces using microwave plasma chemical vapour deposition
122	(MPCVD), Figure 1.
123	Coating was carried out using a computer-controlled 2.45 GHz microwave generator
124	(variable power output – maximum 1000 Watts), TE ₀₁ single mode cavity (Sairem
125	downstream plasma source WR340), double plunge microwave tuner, mass-flow controllers
126	(MFC) and a carrier (Argon) and precursor gas at a total flow rate of 50 cm ³ min ⁻¹ . Sample
127	coatings were made at methane concentrations of 2, 10 and 20% for $^{12}CH_4$ and 2% for $^{13}CH_4$.
128	For coating, each cylindrical PGA graphite disc was placed on a glass sinter situated inside a
129	quartz tube which was aligned to position the disc within the centre of the waveguide. The
130	tube was then connected to the mass-flow controllers, a gas flow was established and then the
131	system was placed under a low vacuum. Once a 1000 Pa system pressure had been achieved
132	the microwave generator was switched on and the microwave reflectance was reduced, as
133	much as possible, using the double plunge microwave tuner. Once the microwave reflectance
134	was tuned the CVD coating process was left to proceed for a period of 30 minutes [20].
135	Additionally, deposition was performed at varying pressures (1000, 5000, 10 000 Pa),
136	however a flow rate of 50 cm ³ min ⁻¹ for the gas mixture did not achieve a system pressure of
137	less than 700 Pa. A lower flow rate of 20 cm ³ min ⁻¹ was applied at 10% ¹² CH ₄ so that a
138	system pressure of 500 Pa could be achieved, additionally growth was performed at 10 Pa
139	system pressure at this reduced flow rate.
140	1-2 mm particles were also produced alongside the disc samples due to crucible size
141	restrictions for the Linkam catalyst stage for Raman spectroscopy. Additional PGA graphite
142	was provided by the National Nuclear Laboratory (NNL). This graphite was sectioned into
143	smaller rectangular sheets using a JCB toolbox saw and then cut into smaller monoliths using
144	an Erbauer ERB180C tile cutter (with no coolant) thus making the graphite more
145	manageable. The graphite monoliths were then put into a metal container and placed into a
146	10-ton hydraulic press, where a pressure between 5-10 tonnes of pressure was used to break
147	the graphite down into smaller pieces. The pieces were then subsequently filtered using a 3
148	compartment Fisherbrand stainless steel sieve (aperture sizes: >2 mm, 1-2 mm and <1 mm)
149	and the 1-2 mm particles were retained for subsequent microwave deposition. Both the larger
150	and smaller pieces were repeatedly pressed until all of the graphite was left as a mixture of
151	either particles or powder, following sieving.

152	A selection of virgin PGA samples (i.e. without deposit) and irradiated graphite specimens
153	extracted by trepanning from a Magnox power station were also analysed for comparison,
154	exact details previously described in [4].
155	2.2. Scanning electron microscopy/ Focused ion beam
156	A Helios NanoLab 600i combined SEM/FIB system (FEI, Oregon USA) was used to obtain
157	scanning electron micrographs. The focused ion beam (FIB) was utilised to precision mill
158	trenches to allow the thickness and morphology of the deposit to be determined with
159	nanometre accuracy and to allow subsequent analysis using other techniques.
160	Electron micrographs were acquired using an accelerating voltage of 15 kV, an electron bean
161	current of 0.17 nA and a dwell time of 100 µs. Trenches were FIB milled with the use of a
162	Ga ⁺ ion source with an accelerating voltage of 30 kV. A Selective Carbon Mill (SCM) gas
163	was used throughout to enhance milling rates. The SCM admits small amounts of water
164	vapour directly over the milling area, promoting gasification of the milled material,
165	enhancing the etch rate and reducing redeposition. It also minimises beam damage and
166	therefore reduces the need to deposit platinum on the surface as a protective measure.
167	Initially a 20 nA beam current was used to generate coarsely defined trenches, with
168	subsequent incremental reductions in ion current to reach a final beam current of 0.9 nA for
169	surface finishing. The milled trenches had approximate dimensions of 50 μ m x 56 μ m x 20
170	μm (x, y and z respectively). The trench faces were smooth and flat, allowing for direct and
171	high spatial resolution observation of structures and features.
172	2.3. Magnetic Sector-Secondary Ion Mass Spectrometry
173	For isotopic analysis of the samples, an in-house built magnetic sector secondary ion mass
174	spectrometer (MS-SIMS) was utilised. Full details of the system are described elsewhere
175	[21]. In summary the system comprised of a focused gallium ion gun (FEI electronically
176	variable aperture type) fitted to a Vacuum Generators model 7035 double-focusing magnetic
177	sector mass analyser with a channeltron detector. The sample was held at a 4 kV potential
178	during analysis. The equipment was controlled using PISCES software, written in-house by
179	Dayta Systems Ltd (Thornbury, UK). The system was capable of providing selected ion
180	mapping and depth profiling with sub-micron resolution.
181	MS-SIMS analyses were performed in negative ion mode for both spectral acquisition and
182	secondary ion imaging. Mass spectra and depth profiles were initially acquired from 4

183	different areas of the 2% 12 C and 13 C methane deposits, detecting mass/charge (m/z) signals
184	at 12, 13, 24 and 26 Da. These ion signals are generated due to the C^- and C_2^- ions derived
185	from sputtered ¹² C and ¹³ C respectively. Mass spectra were obtained by scanning through the
186	mass range 0-100 Da in 0.05 Da steps, with duration of 100 ms per step and 200 s in total.
187	Data acquisition was performed at a low magnification to reduce beam damage (area
188	analysed ~0.25 mm ²) and with a 3 nA beam current. Identification and calibration of the
189	exact m/z values for use in subsequent depth profiles and images were achieved with the use
190	of these survey spectra.
191	Depth profiles record the ion yield intensity from selected sputtered analyte ions over time
192	while rastering the ion beam over a selected area. As the deposits are suitably thick it is not
193	anticipated that the depth profile will sputter enough material to immediately expose the
194	underlying graphite. This allows the signal to be averaged over a set period of time and then
195	the ratio between signals to be compared. Depth profiles were acquired for 1800 s with a
196	beam current of 3 nA and area analysed of approximately 2500 μm^2 . Electronic gating was
197	used throughout to eliminate signal created at the margins of the etched area. Signal averages
198	and ratios were calculated from 200 s to 1800 s, disregarding the first 200 s of data as this
199	was the observed transient period for the experiment.
200	The species compared were the C_2^- ions at 24 and 26 Da, rather than 12 and 13 Da, due to the
201	strong signals obtained from these species, and also to avoid some prominent mass
202	interferences. Interference peaks are difficult to eliminate, however the use of the C_2^- peak is
203	appropriate as the present work is not trying to identify trace elements but aiming to
204	investigate whether the surface deposits are formed of ¹³ C, to what extent ¹³ C is incorporated
205	into the graphite and how thick the overall deposit is.
206	Secondary ion images were recorded from the FIB milled trenches using the C_2^- ions (24 and
207	26 Da). The images were obtained by selecting the m/z ratio of the ion of interest, and then
208	raster scanning the ion beam over a defined area of the sample. The images presented in this
209	paper were acquired over a total area of approximately 0.0225 mm ² . Each image was
210	acquired over a 60 second period using a 0.3 nA beam current to give the best possible spatial
211	resolution whilst still maintaining sufficient ion signal.
212	2.4.Catalyst stage Raman spectroscopy

7

A CCR1000 catalyst stage reactor system connected to a T95 system controller and LinkPad

interface (Linkam, Surrey UK) was used for the thermal oxidation of the PGA graphite 1-2

213

215	mm particles. For in situ spectral acquisition, a LabRAM HR800 confocal Raman microscope
216	(Horiba Jobin Yvon, Kyoto Japan) was used. The sample was heated up in the crucible inside
217	of the catalyst stage from room temperature up to 600 °C (at 10 °C min ⁻¹), with a 50 cm ³ min ⁻¹
218	¹ flow of air. Spectra were acquired using a 532 nm laser, a 50X long-working distance
219	objective, a 300 g mm ⁻¹ grating, and spectral acquisition times of 25 s every 50 °C.
220	The heating regime and the spectral acquisition parameters for automated analysis were
221	controlled using a built-in Linkam module script in the Horiba Labspec 6 software package.
222	The Raman spectroscopy system was calibrated using the 520 cm ⁻¹ peak from a silicon
223	crystal.Spectral analysis, during thermal oxidation in air, of virgin PGA graphite and PGA
224	graphite with ¹² C and ¹³ C carbonaceous deposits was carried out to analyse the thermal
225	profile of the surface material (i.e. graphite substrate) and the "cauliflower-like"
226	carbonaceous deposit. This technique allows for analysis of the thermal oxidation
227	properties/reactivity of the different carbon materials and also surface chemical changes due
228	to thermal oxidation.
229	3. Results
230	3.1. Scanning Electron Microscopy
231	The deposit formed on irradiated graphite taken from Oldbury Magnox reactor has a distinct
232	and pronounced morphology, Figure 2a, compared to virgin PGA graphite, Figure 2b [3]. For
233	comparison, electron micrographs of the 2% $^{12}\mathrm{CH_4}$ and 2% $^{13}\mathrm{CH_4}$ deposits can be seen in
234	Figure 3, a and b respectively. The distinction between deposit and underlying graphite
235	should be noticeable due to the lack of characteristic features in the deposit that are routinely
236	seen in all PGA graphite such as shrinkage cracks and ligaments between pores [22], Figure
237	4. The deposits found on irradiated graphite have a 'cauliflower-like' appearance due to an
238	agglomeration of irregular spheres, Figure 5. After FIB milling the internal morphology of
239	the 2% $^{13}\text{CH}_4$ and 2%, 10% and 20% $^{12}\text{CH}_4$ deposited samples can be seen in Figure 6a, b ,c
240	and d respectively.
	The 2011 12 of 13
241	The 2% ¹² C and ¹³ C methane CVD deposits were observed to have a porous, 'feathery'
242	texture that appears to be significantly less dense than the underlying graphite. For the
243	irradiated graphite however, there was very little distinction in density or fine structure
244	between the deposit and the underlying graphite (the deposit appears to have a lower porosity
245	compared to virgin PGA, Figure 5). It is possible that the underlying PGA graphite in the

irradiated samples is protected from radiolytic oxidation by the carbon deposit, leading to the deposit and underlying graphite being difficult to distinguish [15].

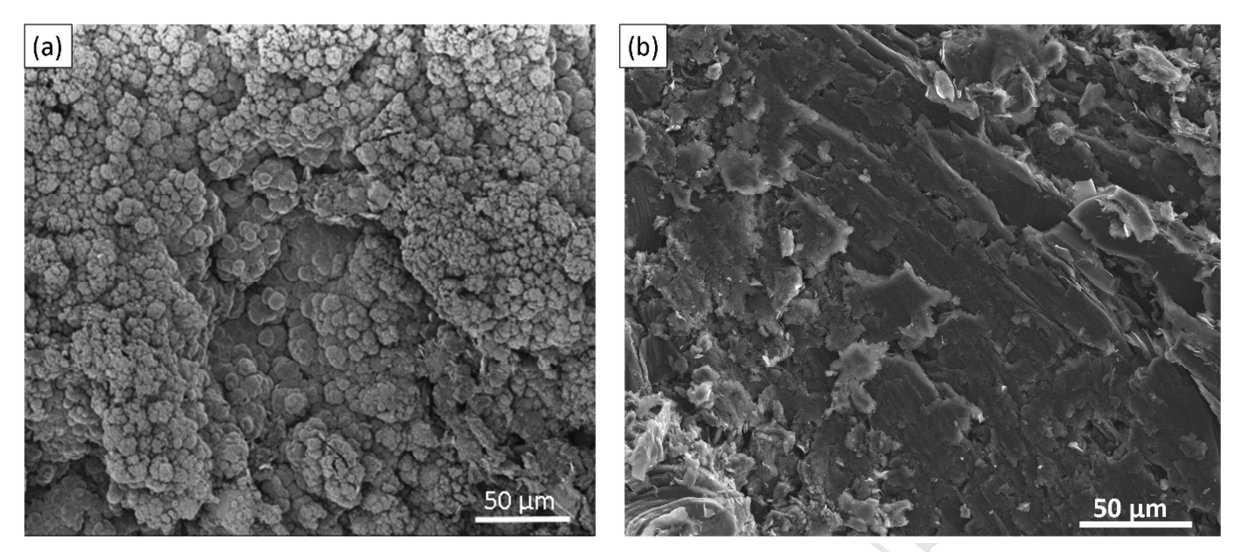


Figure 2,a) Focused ion beam mage of deposit found on irradiated graphite surface, from [4] and b) virgin PGA surface.

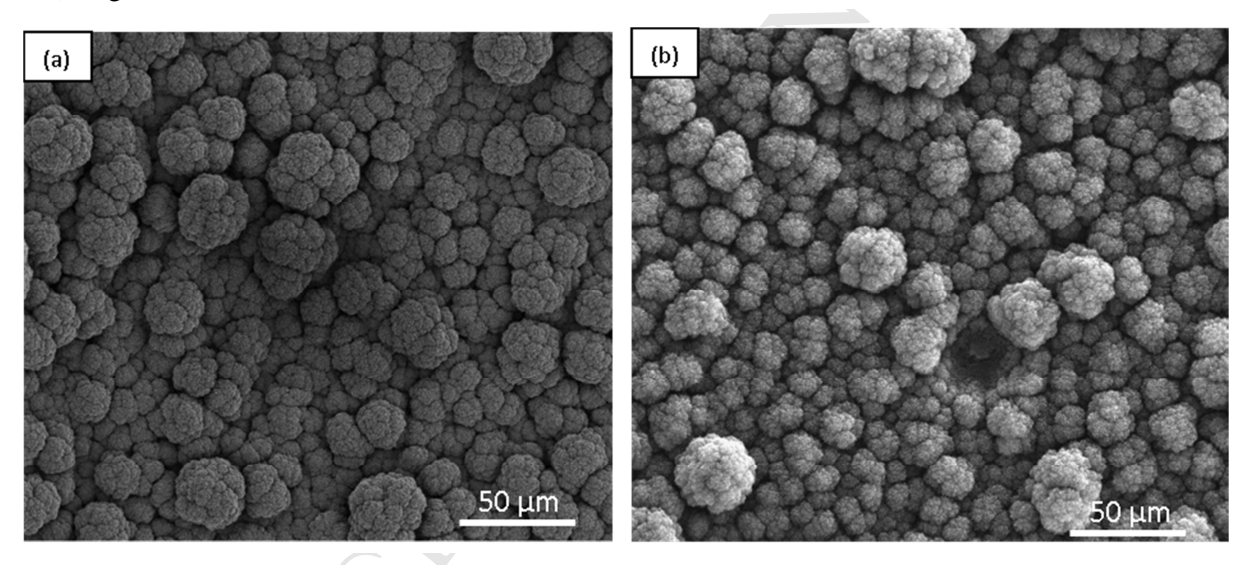


Figure 3, Scanning electron micrographs from ¹²C (a) and ¹³C (b) carbonaceous deposits on Pile Grade A graphite, system pressure 1000 Pa.

Further investigation using greater methane concentrations showed increases in the apparent density of the deposit (which was only determined visually), Figures 6 (b), (c) and (d), that are more closely comparable to the deposit found on irradiated graphite. Deposits produced at system pressures of 5000 and 10000 Pa were of different morphology, instead comprising an agglomeration of spherical deposits that were not as extensive or as thick as those grown at the lower pressure of 1000 Pa. Reducing the flow rate to 20 cm³ min ⁻¹ allowed a system pressure of 500 Pa to be achieved, however even though the surface topography of the

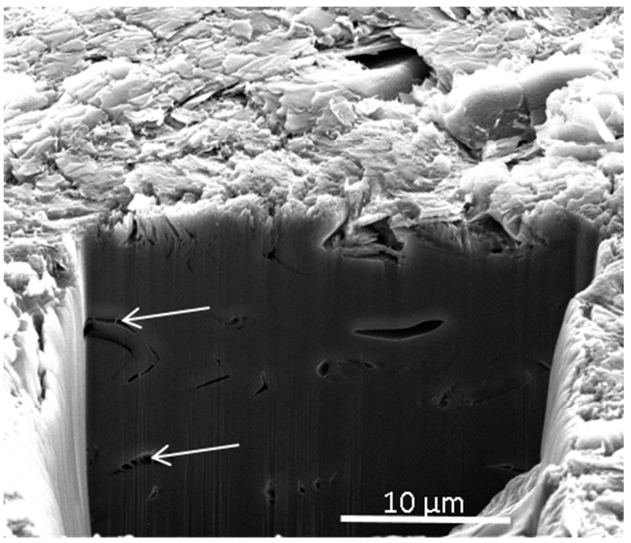


Figure 4, Scanning electron micrograph from cross section of an uncoated Pile Grade A graphite after FIB milling showing characteristic cracking and ligaments, shown with the arrows.

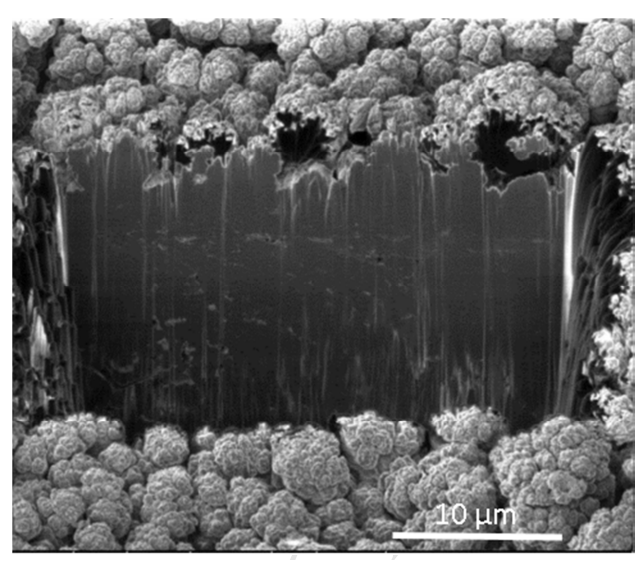


Figure 5, Focused ion beam image from cross section of channel wall trepanned sample from a Magnox reactor [3].

deposit was similar to irradiated material and the other cauliflower-like deposits formed, the internal morphology exhibited extensive porosity and this did not appear suitable as a simulant, Figure 7(a). Conversely, growth at a system pressure of 1000 Pa at this reduced flow rate formed a deposit that was very similar to that grown at 50 cm³ min⁻¹, Figure 7(b). The deposit formed at 1000 Pa pressure at 10% methane concentration showed the closest resemblance to those seen on Oldbury irradiated Magnox graphite and was deemed to be the most suitable for use as a simulant.

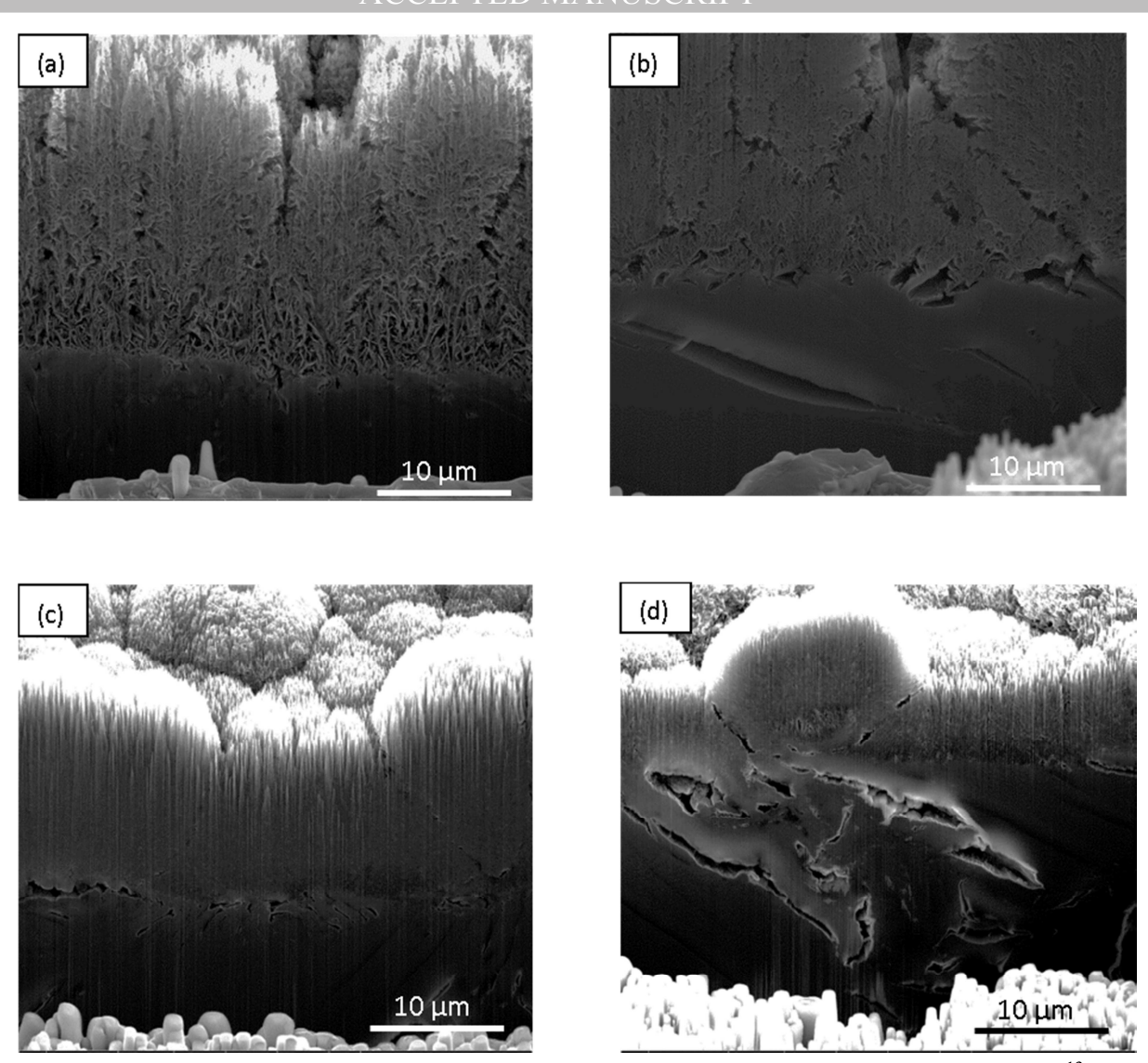


Figure 6. Scanning electron micrographs showing the ion beam milled cross sections for 2% $^{13}CH_4$ (a) and 2% (b), 10% (c) and 20% (d) $^{12}CH_4$ deposited samples, all at system pressure of 1000 Pa.

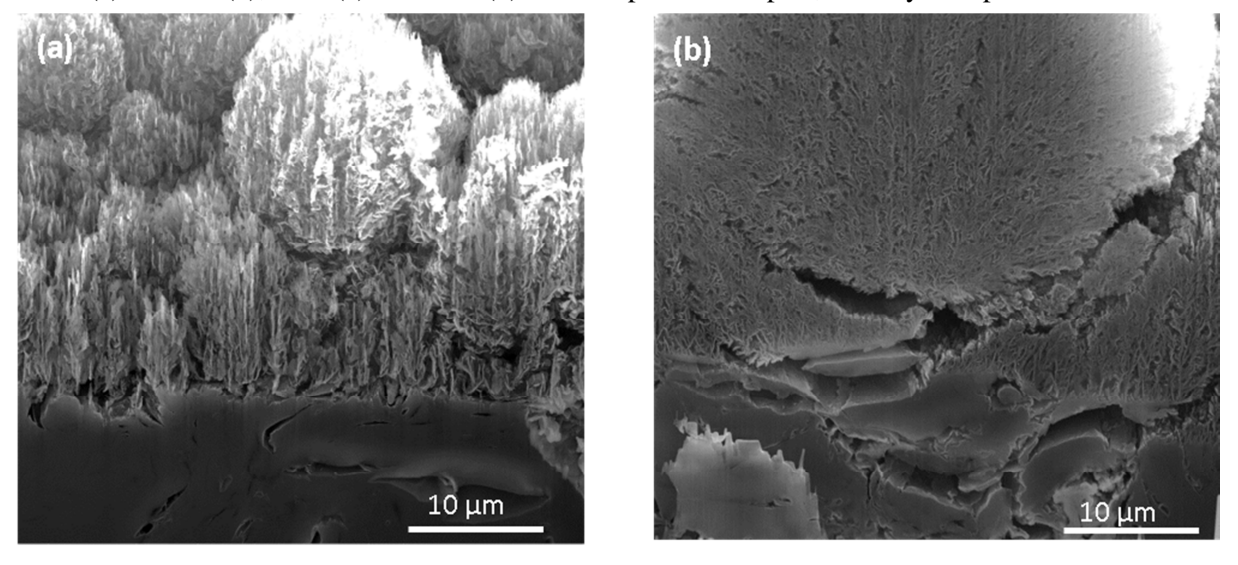
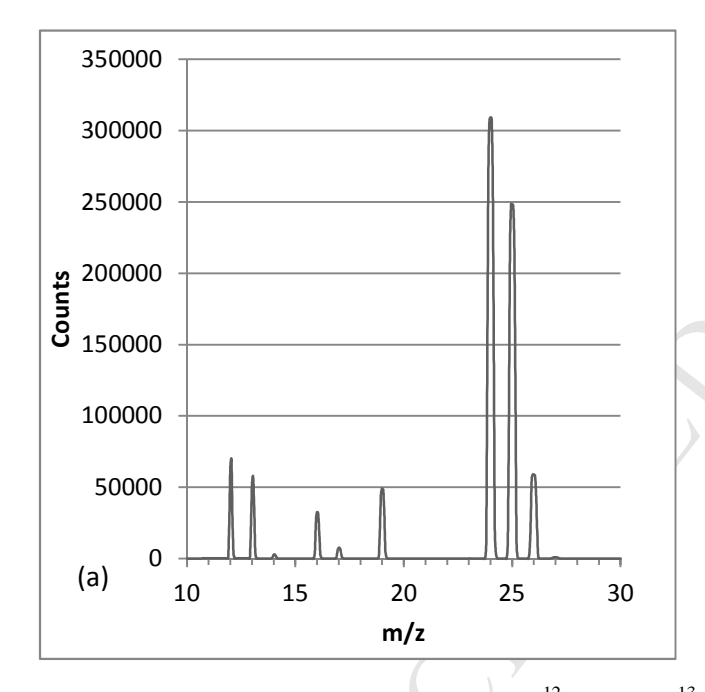


Figure 7. Scanning electron micrographs showing the ion beam milled cross sections at system pressures of 500 (a) and 1000 (b) Pa, flow rate $20~\text{cm}^3~\text{min}^{-1}$.

3.2. Secondary Ion Mass Spectrometry

Survey spectra from the 2% methane 12 C and 13 C deposits are shown in Figures 8 (a) and (b) respectively. Signals recorded at mass/charge peaks of 13 Da (13 C $^-$ and 26 Da (13 C $_-$)) are significantly greater in the 13 C deposit compared to the 12 C deposit, although these signals are also present in the 12 C sample due to 12 CH $^-$ and 12 CN $^-$ species respectively. The mean ratio (n=4) between the peak heights at 26 Da and 24 Da for the 12 C deposit was found to be 0.14 \pm 0.03. The mean ratio (n=4) for the 13 C deposit was 115.3 \pm 19.1. This increase of several orders of magnitude is strong evidence that the deposit is predominately 13 C as the interfering peak from 12 CH at 13 Da is unlikely to be higher in the 13 C sample. The errors given here are likely to be due to the strong dependence of signal intensity on location and geometry of the sample in the SIMS system [23].



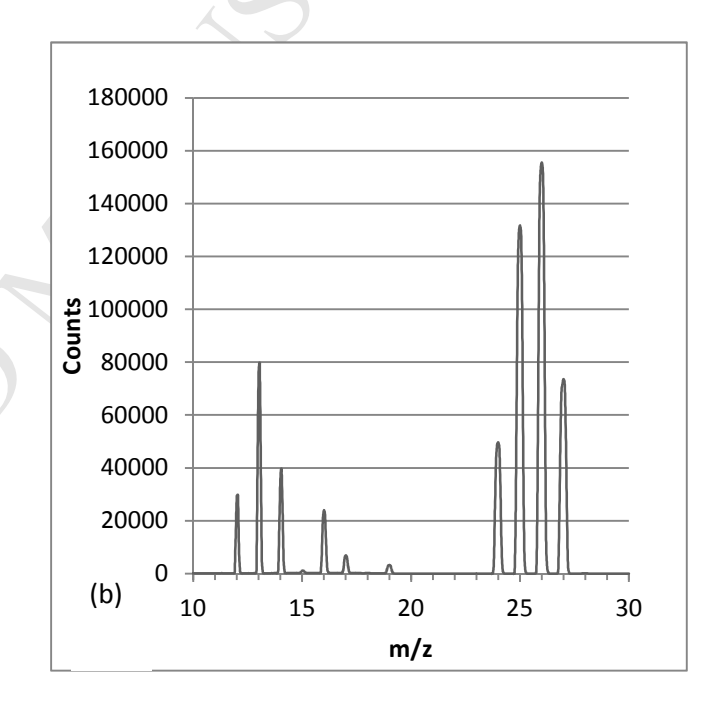


Figure 8, SIMS spectra from 2% methane ¹²C (a) and ¹³C (b) deposit.

The areas analysed were selected randomly and the only criteria for examination was that 283 they produced sufficient SIMS signal to allow analysis. Due to the surface not having a 284 uniform, flat surface there are likely to be topographic effects that will affect the signal 285 recorded. This has been studied by other authors [23-25] with suggestions that the changes 286 may be due to the incident angle of the beam, the height of the features and variations in the 287 electric field due to topographic features that may lead to trajectory changes of the secondary 288 ions [24]. 289 SIMS ion signal maps have been recorded for 26 Da and 24 Da for a ¹³C sample, Figure 9 (a) 290 and Figure 9 (b) respectively. For the ¹³C deposit the mass peak signal at 26 Da is present 291 primarily on the deposit with a significant reduction in signal in the underlying graphite with 292 the 24 Da signal being the reverse, with a more intense signal recorded in the underlying 293 graphite than in the deposit. This shows that the ¹³C is deposited on top of the underlying 294 graphite. The signal at the bottom of the trench has a relatively high intensity for both 24 and 295 26 Da, and this may be due to re-deposition of sputtered material originating from the ¹³C 296 deposit during FIB milling of samples [26]. 297

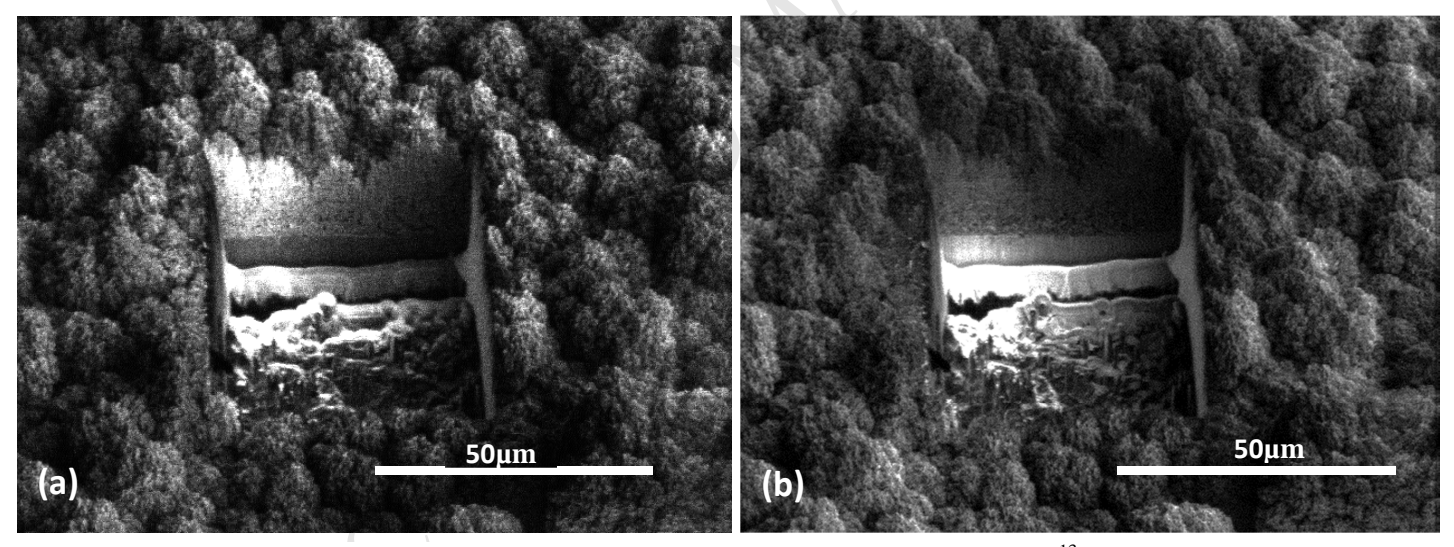


Figure 9, Secondary Ion signal maps for 26 Da (a) and 24 Da (b) from cross section of ¹³C carbonaceous deposit on top of Pile Grade A graphite after FIB milling.

3.3. Catalyst stage Raman spectroscopy

298

299

300

301

302

A three-vectored graph displaying Raman shift, intensity and temperature (x, y and z axis respectively) was used to illustrate the Raman spectra at each temperature during the thermal oxidation experiment. The Raman spectra are displayed between $1100 - 1700 \, \text{cm}^{-1}$ to allow the critical peaks related to both ^{12}C and ^{13}C carbonaceous materials to be compared. The ^{12}C

peaks are the ¹²D peak at ~1350 cm⁻¹ and the ¹²G peak at ~1575 cm⁻¹ and the ¹³C peaks are the 13 D peak at ~1300 cm $^{-1}$ and the 13 G peak at ~1525 cm $^{-1}$.

Virgin PGA 3.3.1.

The thermal oxidation spectral profile for a virgin PGA graphite 1-2 mm particle is shown in Figure 10. This spectral profile shows that there was a negligible change in the intensity of the D and G peaks between 50 - 600 °C. This indicates that between 50 - 600 °C the surface of the PGA graphite undergoes very minimal surface oxidation and that the PGA is mostly unreactive. As the surface of the virgin PGA material remains relatively unchanged during thermal oxidation it will readily allow for any spectral changes, due to the thermal oxidation of ¹²C

and ¹³C carbonaceous deposits, to be isolated.

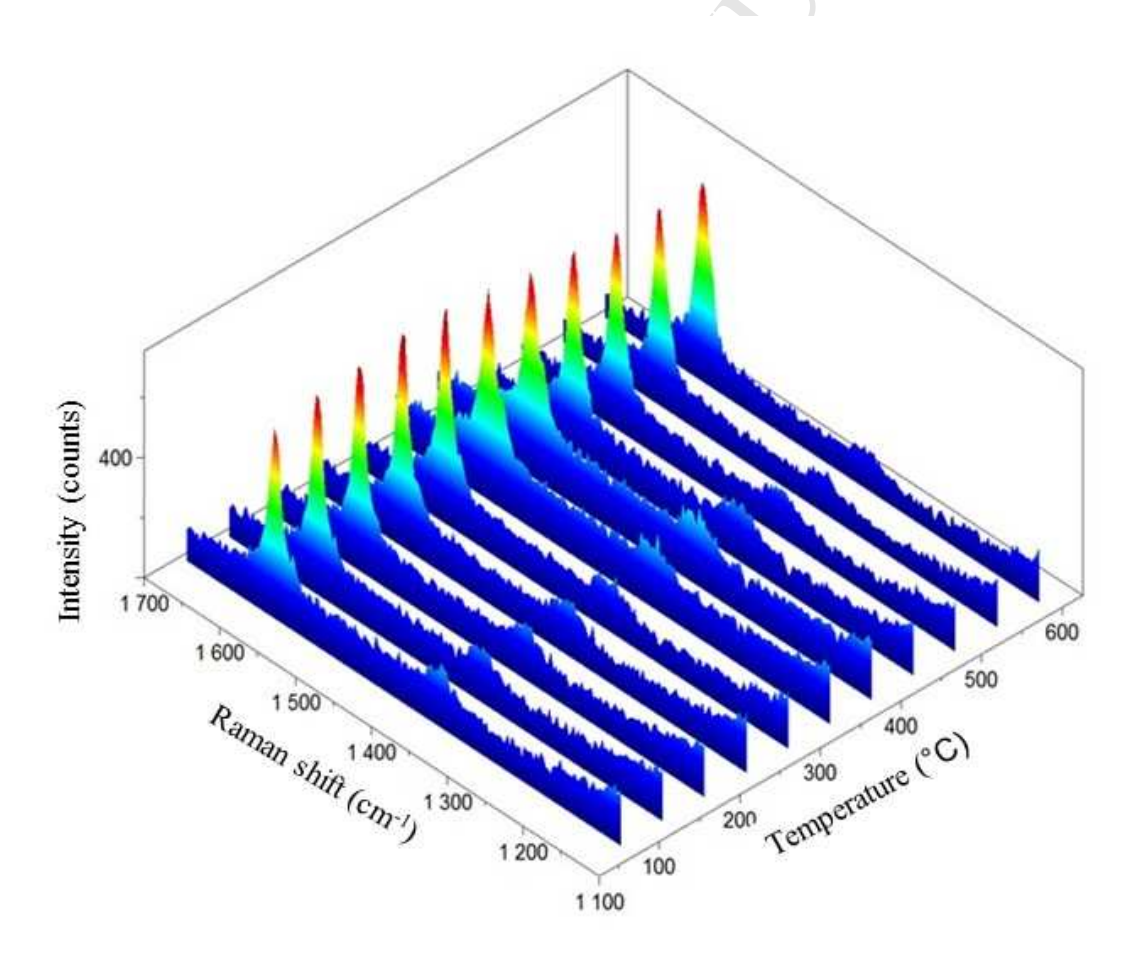


Figure 10, In situ Raman spectral analysis, during thermal oxidation, of a 1-2 mm virgin PGA graphite particle.

314

303

304

305

306

307

308

309

310

311

312

3.3.2. PGA Graphite with ¹²C and ¹³C Deposits

The thermal oxidation spectral profiles for a 2 % 12 CH₄ and 13 CH₄ deposit on a PGA graphite particle are shown in Figures 11 and 12 respectively. Figure 11 shows that there is a noticeable decrease in the 12 D peak intensity between 400 – 600 °C. This indicates that the 12 C carbonaceous deposit begins to thermally oxidise at approximately 400 °C and appears to have been completely removed by 600 °C indicated by the intensity of the 12 D peak at 600 °C, showing the spectral profile of the virgin PGA graphite material. There is a noticeable decrease in the 13 D & 13 G peak intensities between 450 – 600 °C in Figure 12, which are solely present due to the 13 C carbonaceous deposit. This indicates that the 13 C carbonaceous deposit begins to thermally oxidise at approximately 450 °C and appears to have been completely removed by 600 °C indicated by the absence of the 13 D &

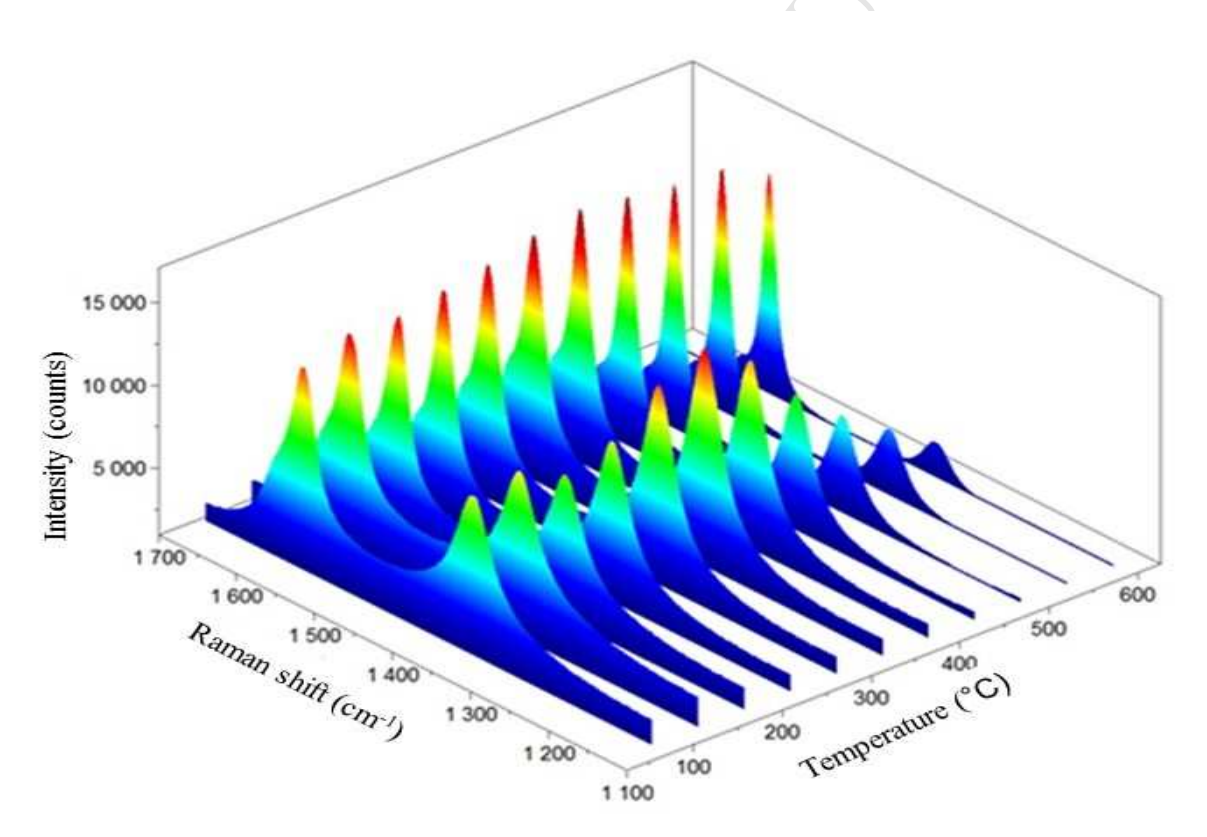


Figure 11, $In\ situ$ Raman spectral analysis, during thermal oxidation, of a 2% CH₄ 12 C carbonaceous deposit on a 1-2 mm PGA graphite particle

¹³G peaks at 600 °C, showing the spectral profile of the virgin PGA graphite material. The intensities of the ¹²D and ¹²G peaks (PGA graphite) do not decrease but in fact increase relative to the decrease in the intensities of the ¹³D and ¹³G peaks (¹³C carbonaceous

communication, 11th November 2013).

deposit), which also illustrates that the surface of the virgin PGA material, as a base substrate, remains relatively unchanged during thermal oxidation.

As the Raman peaks associated with the deposits decrease between 400 - 600 °C it indicates that the carbonaceous material on the surface has a similar oxidation temperature to that of the carbonaceous deposits found on irradiated PGA graphite (M. P. Metcalfe, personal

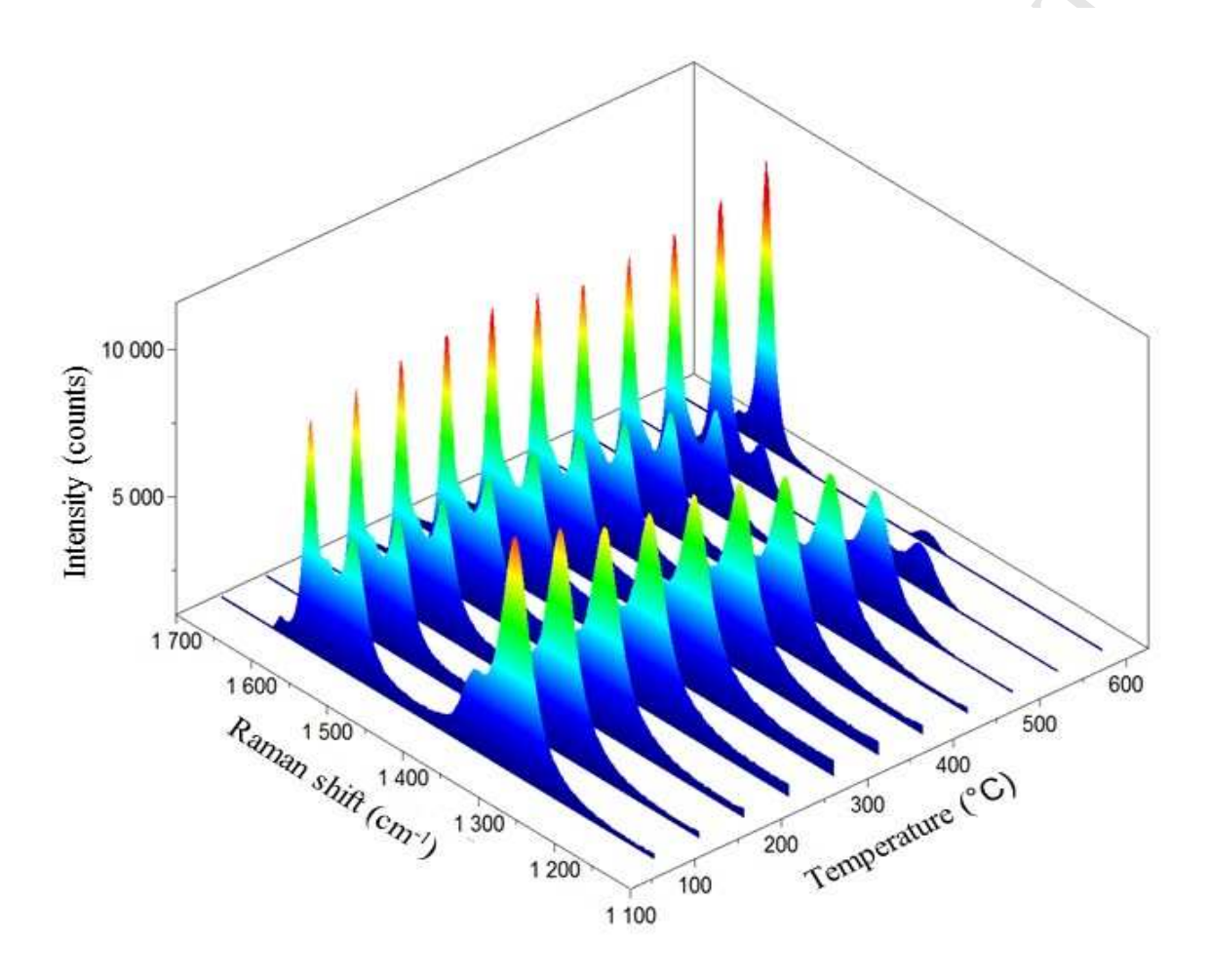


Figure 12, *In situ* Raman spectral analysis, during thermal oxidation, of a 2% CH₄ ¹³C carbonaceous deposit on a 1-2 mm PGA graphite particle

Figure 13 illustrates the isothermal profiles of virgin PGA graphite, irradiated PGA graphite deposit & a ¹²C microwave simulant deposit at 450 °C, in air, over a 50 hour period. The oxidation of virgin PGA graphite is negligible whereas the irradiated PGA graphite deposit & the C-12 microwave simulant deposit show significantly greater rates of oxidation and are clearly more reactive. Initially the rates of thermal oxidation remain fairly similar for the first 5 hours for the irradiated PGA graphite deposit & the ¹²C microwave simulant deposit but for the next 45 hours the irradiated PGA graphite deposit shows a greater rate of thermal

oxidation. This deviation in rates of reactivity may be due to irradiated damage caused to the underlying PGA graphite in the irradiated PGA graphite sample whereas the underlying PGA graphite in the microwave simulant underwent no irradiation and started off as pristine virgin PGA graphite. However the microwave simulant carbonaceous deposit reactivity seen in the TGA isothermal data shows a similar reactivity to that of the carbonaceous deposit seen in irradiated PGA graphite.

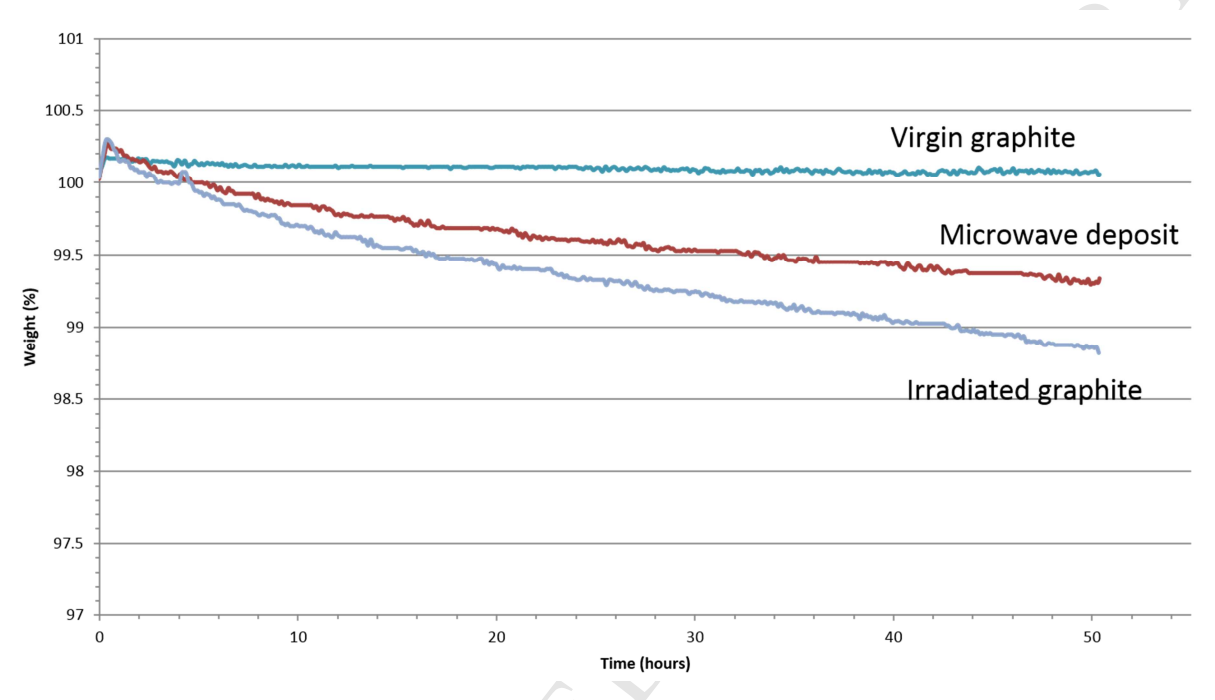


Figure 13, Thermograms from virgin PGA graphite, irradiated PGA graphite and ¹²C simulant deposit on PGA graphite examined at 450 °C, in air, over a 50 hour period.

4. Discussion

Previous examination [3] of irradiated graphite from Magnox reactors has shown that during generation lifetime a carbonaceous deposit can be formed on the fuel and interstitial channel walls of the graphite moderator that has a markedly different morphology to the underlying PGA graphite. This work aimed to form a similar carbonaceous deposit using ¹³C precursor gas to allow subsequent investigation of the behaviour of such deposits in leaching and microbial studies pertinent to examining graphite degradation and ¹⁴C release in a GDF [27]. Use of a simulant allows future experiments to be performed more easily than using irradiated graphite due to a removal of the need to work with radioactive materials. However, the use of simulants necessitates care to ensure that they are representative of the properties being examined. With the use of several experimental techniques (FIB, SEM, MS-SIMS, Raman) this work has examined the internal morphology as well as the surface

360	topography of carbonaceous deposits formed using microwave plasma CVD and compared
361	them to irradiated graphite trepanned from a Magnox power station graphite core.
362	Microwave plasma CVD has been used to form adherent carbonaceous deposits on the
363	surfaces of virgin (unirradiated) PGA graphite discs. Microwave plasma CVD is widely used
364	to grow other carbon materials with differences in growth parameters (precursor gas,
365	temperature, pressure, microwave power) leading to different allotropes being formed most
366	notably Carbon-Nanotubes (CNT) [28, 29] and diamond [30, 31]. Initially, ¹² C precursor gas,
367	using a system pressure of 1000 Pa with a flow rate of 50 cm ³ min ⁻¹ , was used, primarily due
368	to the high cost of labelled isotopic gases, and with the use of scanning electron microscopy
369	the surface topography was found to be very similar to the 'cauliflower-like' deposits found
370	on irradiated graphite [3]. However, after sectioning with a focused ion beam it was found
371	that the internal morphology was more porous than the deposit found on irradiated graphite.
372	This is believed to be due to the growth rate, approximately 50 µm hour ⁻¹ , of the deposit
373	being too rapid to allow a dense deposit to be formed. By comparison, growth rates of
374	diamond using microwave plasma CVD are usually in the region of 1 μm hour $^{-1}$ [32] and
375	these form 'solid' deposits. By increasing the methane concentration in the precursor gas mix
376	an increased density in the deposit was achieved, likely due to the increased availability of
377	carbon radicals available for deposition. It should be noted that the deposits formed on
378	irradiated graphite are formed at conditions that are very difficult to replicate, pressures of 1-
379	3 MPa, temperatures of approximately 400 °C and in the presence of a neutron flux [33],
380	therefore the high density of the deposits found on irradiated graphite is likely due to the high
381	pressure environment, whereas in microwave plasma CVD low pressures are used so that the
382	plasma can be sustained.
383	Further experiments were carried out to investigate the parameters which can affect the
384	growth rate of carbonaceous deposits and to determine whether a more representative
385	carbonaceous deposit could be formed using microwave plasma CVD. Experiments carried
386	out at 200 W using 2, 10 & 20% CH ₄ failed to generate carbonaceous deposits. However,
387	deposition at 400 W induced a rapid growth of carbonaceous material.
388	Further tests were carried out at both 5000 & 10000 Pa pressures using 10% CH ₄ . Deposits
389	were produced for both pressures; however these deposits showed a thin agglomeration of
390	carbonaceous spheres on the graphite substrate. This difference in form and thickness shows
391	that growth at higher pressures is not suitable in producing an analogous material for studying
392	irradiated material. At pressures of 500 Pa with the reduced flow rate the deposit was not
393	analogous of those found in irradiated material, suggesting that the most representative

394	deposit is formed at system pressure of 1000 Pa with a 50 cm ³ min ⁻¹ flow of 10% CH ₄ :90%
395	Ar.
396	Growth using ¹³ C precursor gas showed a similar topography/morphology to ¹² C deposits
397	indicating that there is no appreciable difference in the growth mechanism between the
398	different isotopes, thereby justifying the use of this simulant to study the behaviour of
399	carbonaceous deposits found on irradiated graphite. The clear separation of the deposit and
400	underlying graphite shown by isotopic imaging using a MS-SIMS has shown that a deposit is
401	formed, and cross-sectional images indicate that the topography and morphology are very
402	similar to the ones found on irradiated graphite. Catalyst stage Raman spectroscopy
403	combined with TGA have shown these deposits to be of a similar reactivity to those found on
404	irradiated graphite. These deposits appear to be suitable for further studies involving
405	microbial systems to examine the possible release of the deposit into the environment in a
406	geological disposal facility. Based on the thermal oxidation behaviour, the density difference
407	in the surface deposit materials between irradiated and simulant samples does not appear to
408	significantly influence observed reactivity. With the surface layers exhibiting rapid
409	degradation at much lower temperatures than the underlying graphite.

5. Conclusion

410

414

415

416

417

418

419

420

421

- Carbonaceous ¹²C and ¹³C deposits were formed on Pile Grade A graphite using microwave plasma deposition and examined using Focused Ion Beam, Scanning Electron Microscopy and Magnetic Sector-Secondary Ion Mass Spectrometry. Several conclusions can be drawn:
 - 1. The surface topography of both ¹²C and ¹³C deposits formed by MPCVD are very similar to the 'cauliflower-like' deposits found on graphite samples trepanned from a Magnox reactor.
 - 2. Deposits formed at 1000 pa system pressure with a 50 cm³ min⁻¹ flow of 10% CH₄:90% Ar showed the closest resemblance to the deposits on the irradiated material.
 - 3. The internal morphology of the deposit is slightly more porous than that found in irradiated graphite. However, variations in methane concentrations and gas pressure can affect the density of deposited material.
- To summarise, there is a potential use of the ¹³C containing deposits synthesised in this work to act as simulants in future studies aimed at better understanding and predicting the post-

- disposal behaviour of irradiated graphite waste in a geological disposal environment and the
- 426 associated release profile of ¹⁴C arising from the labile deposit.

427 **Acknowledgements**

- The authors would like to thank the EPSRC and Radioactive Waste Management for the
- funding of this work (The post-disposal Behaviour of C-14 and Irradiated Graphite [BIG],
- 430 Grant No EP/1036354/1). The support of our co-workers at the University of Huddersfield
- (www.hud.ac.uk/c-14-big) and advice from colleagues in Magnox Ltd and the National
- 432 Nuclear Laboratory is also gratefully acknowledged.

433 References

- 434 [1] Nuclear Decommissioning Authority. Higher Activity Waste, The Long-term Management of
- 435 Reactor Core Graphite Waste Credible Options (Gate A), SMS/TS/D1-HAW-6/002/A 2013.
- 436 [2] Nuclear Decommissioning Authority. Geological Disposal, Carbon-14 Project Phase 1
- 437 Report, NDA/RWMD/092 2012.
- 438 [3] Heard PJ, Payne L, Wootton MR, Flewitt PEJ. Evaluation of surface deposits on the channel
- wall of trepanned reactor core graphite samples. Journal of Nuclear Materials. 2014;445(1–3):91-7.
- 440 [4] Payne L, Heard, P. J, Scott T. B. Enrichment of C-14 on Surface Deposits of Oldbury Reactor
- 441 Graphite Investigated with the Use of Magnetic Sector Secondary Ion Mass Spectrometry Waste
- 442 Management Symposia 2015 Proceddings. 2015.
- 443 [5] Hou X. Rapid analysis of 14C and 3H in graphite and concrete for decommissioning of
- nuclear reactor. Applied Radiation and Isotopes. 2005;62(6):871-82.
- 445 [6] Baston G, Marshall T, Otlet R, Walker A, Mather I, Williams S. Rate and speciation of volatile
- carbon-14 and tritium releases from irradiated graphite. Mineralogical Magazine. 2012;76(8):3293-
- 447 302.
- 448 [7] Malesevic A, Vizireanu S, Kemps R, Vanhulsel A, Haesendonck CV, Dinescu G. Combined
- growth of carbon nanotubes and carbon nanowalls by plasma-enhanced chemical vapor deposition.
- 450 Carbon. 2007;45(15):2932-7.
- 451 [8] Bystrov K, Westerhout J, Matveeva M, Litnovsky A, Marot L, Zoethout E, et al. Erosion yields
- of carbon under various plasma conditions in Pilot-PSI. Journal of Nuclear Materials.
- 453 2011;415(1):S149-S52.
- 454 [9] Wang SG, Zhang Q, Yoon SF, Ahn J, Yang DJ, Wang Q, et al. Electron field emission from
- carbon nanotubes and undoped nano-diamond. Diamond and Related Materials. 2003;12(1):8-14.
- 456 [10] McConnell ML, Dowling DP, Pope C, Donnelly K, Ryder AG, O'Connor GM. High pressure
- diamond and diamond-like carbon deposition using a microwave CAP reactor. Diamond and Related
- 458 Materials. 2002;11(3–6):1036-40.
- 459 [11] Castro M, Cuerno R, Nicoli M, Vázquez L, Buijnsters JG. Universality of cauliflower-like fronts:
- 460 from nanoscale thin films to macroscopic plants. New Journal of Physics. 2012;14(10):103039.
- 461 [12] Wickham, AJ, Sellers, RM, Pilkington, NJ. Graphite Core Stability During "Care and
- 462 Maintenance" and "Safe Storage". Vienna, IAEA-TECDOC 1043. 1998.
- 463 [13] Wickham, AJ, Rahmani, L. Graphite dust explosibility in decomissioning: A demonstration of
- 464 minimal risk. Vienna, IAEA-TECDOC-1647. 2010.
- 465 [14] Burcl, R. Characterization, Treatment and Conditioning of Radioactive Graphite from
- 466 Decomissioning of Nuclear Reactors. Vienna, Austria, IAEA-TECDOC-1521. 2006.

- 467 [15] Minshall P, Sadler I, Wickham A. "Radiolytic Graphite Oxidation Revisited". Poster presented
- at' Specialists meeting on graphite moderator lifecycle behaviour. Bath (United Kingdom): IAEA;
- 469 1996.
- 470 [16] Moskovic R, Heard PJ, Flewitt PEJ, Wootton MR. Overview of strength, crack propagation
- and fracture of nuclear reactor moderator graphite. Nuclear Engineering and Design.
- 472 2013;263(0):431-42.
- 473 [17] May PW. Diamond thin films: a 21st-century material. Philosophical Transactions of the
- 474 Royal Society of London Series A: Mathematical, Physical and Engineering Sciences.
- 475 2000;358(1766):473-95.
- 476 [18] Harton SE, Stevie FA, Ade H. Carbon-13 Labeling for Improved Tracer Depth Profiling of
- 477 Organic Materials Using Secondary Ion Mass Spectrometry. J Am Soc Mass Spectrom.
- 478 2006;17(8):1142-5.
- 479 [19] Silbermann G, Moncoffre N, Toulhoat N, Bérerd N, Perrat-Mabilon A, Laurent G, et al.
- 480 Temperature effects on the behavior of carbon 14 in nuclear graphite. Nuclear Instruments and
- 481 Methods in Physics Research Section B: Beam Interactions with Materials and Atoms.
- 482 2014;332(0):106-10.
- 483 [20] Lancashire UoC. Contaminated material patent GB1312312.0. 2013 9th July 2013
- 484 [21] Heard PJ, Feeney KA, Allen GC, Shewry PR. Determination of the elemental composition of
- 485 mature wheat grain using a modified secondary ion mass spectrometer (SIMS). The Plant Journal.
- 486 2002;30(2):237-45.
- 487 [22] Heard PJ, Wootton MR, Moskovic R, Flewitt PEJ. Crack initiation and propagation in pile
- 488 grade A (PGA) reactor core graphite under a range of loading conditions. Journal of Nuclear
- 489 Materials. 2010;401(1-3):71-7.
- 490 [23] Lee JS, Gilmore I, Seah M, Fletcher I. Topography and Field Effects in Secondary Ion Mass
- 491 Spectrometry Part I: Conducting Samples. J Am Soc Mass Spectrom. 2011;22(10):1718-28.
- 492 [24] Kita NT, Ushikubo T, Fu B, Valley JW. High precision SIMS oxygen isotope analysis and the
- 493 effect of sample topography. Chemical Geology. 2009;264(1):43-57.
- 494 [25] Rangarajan S, Tyler BJ. Topography in secondary ion mass spectroscopy images. Journal of
- 495 Vacuum Science & Technology A. 2006;24(5):1730-6.
- 496 [26] Rajsiri S, Kempshall B, Schwarz S, Giannuzzi L. FIB Damage in Silicon: Amorphization or
- 497 Redeposition? Microscopy and Microanalysis. 2002;8(S02):50-1.
- 498 [27] C14-BIG. 2014 [cited; Available from: http://www.hud.ac.uk/c14-big/
- 499 [28] Bower C, Zhou O, Zhu W, Werder DJ, Jin S. Nucleation and growth of carbon nanotubes by
- microwave plasma chemical vapor deposition. Applied Physics Letters. 2000;77(17):2767-9.
- 501 [29] Qin LC, Zhou D, Krauss AR, Gruen DM. Growing carbon nanotubes by microwave plasma-
- enhanced chemical vapor deposition. Applied Physics Letters. 1998;72(26):3437-9.
- 503 [30] Kobashi K, Nishimura K, Kawate Y, Horiuchi T. Synthesis of diamonds by use of microwave
- plasma chemical-vapor deposition: Morphology and growth of diamond films. Physical Review B.
- 505 1988;38(6):4067-84.
- 506 [31] Stoner BR, Glass JT. Textured diamond growth on (100) β -SiC via microwave plasma chemical
- vapor deposition. Applied Physics Letters. 1992;60(6):698-700.
- 508 [32] Yan C-s, Vohra YK, Mao H-k, Hemley RJ. Very high growth rate chemical vapor deposition of
- single-crystal diamond. Proceedings of the National Academy of Sciences. 2002;99(20):12523-5.
- 510 [33] Jensen, SE, Nonbol, E Description of the Magnox Type of Gas Cooled Reactor (MAGNOX),
- 511 NKS/RAK-2(97)TR-C5. 1999.